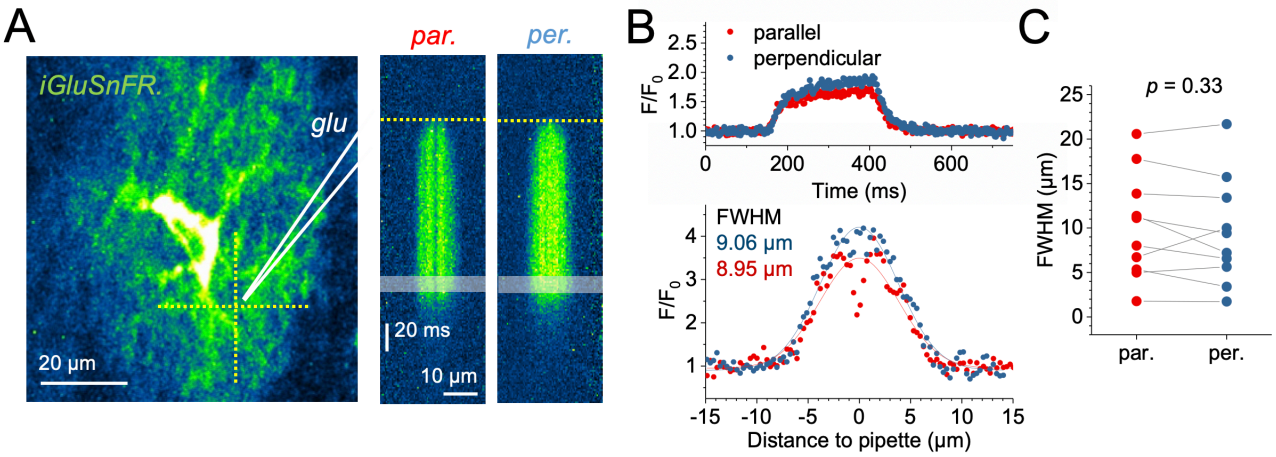

Suppl. Figure 1: Isotropic spread of glutamate visualized by monitoring of iGluSnFr expressed by astrocytes.

Long iontophoretic glutamate applications were used to minimize the potential buffering effect of membrane-anchored iGluSnfr molecules.

(A) Schematic of the experiment (left panel, glutamate iontophoresis pipette in white, iGluSnFR expressing astrocyte in green). Line scans of iGluSnFR fluorescence were obtained in parallel and perpendicular to the CA1 pyramidal layer (left panel, dotted yellow lines) and glutamate was applied for 250 ms (current 10 nA). For analysis and display, the baseline fluorescence intensity (F_0) was determined in a 100 ms time window for each x-coordinate (lane) and the ratio F/F_0 was calculated for each lane (middle and right panel, start of iontophoresis illustrated by yellow dotted lines). iGluSnFR saturation was not observed in these experiments and usually required a much stronger glutamate injection (~100 nA, verified in each experiment).

(B) Example of iGluSnFR fluorescence over time during glutamate application (top panel, averaged over entire line scan). The spatial profile of iGluSnFR fluorescence during the last 20 ms of iontophoresis (shaded area in line scans in **A**) was analysed to estimate the spatial spread of glutamate in both directions. Spatial spread was quantified by the full width at half maximum of a Gaussian distribution fitted to the fluorescence profiles (lower panel).

(C) No statistically significant difference between both directions were observed (n = 10 recordings in 10 different hippocampal slices, parallel and perpendicular line scans always paired, paired Student's t-test).

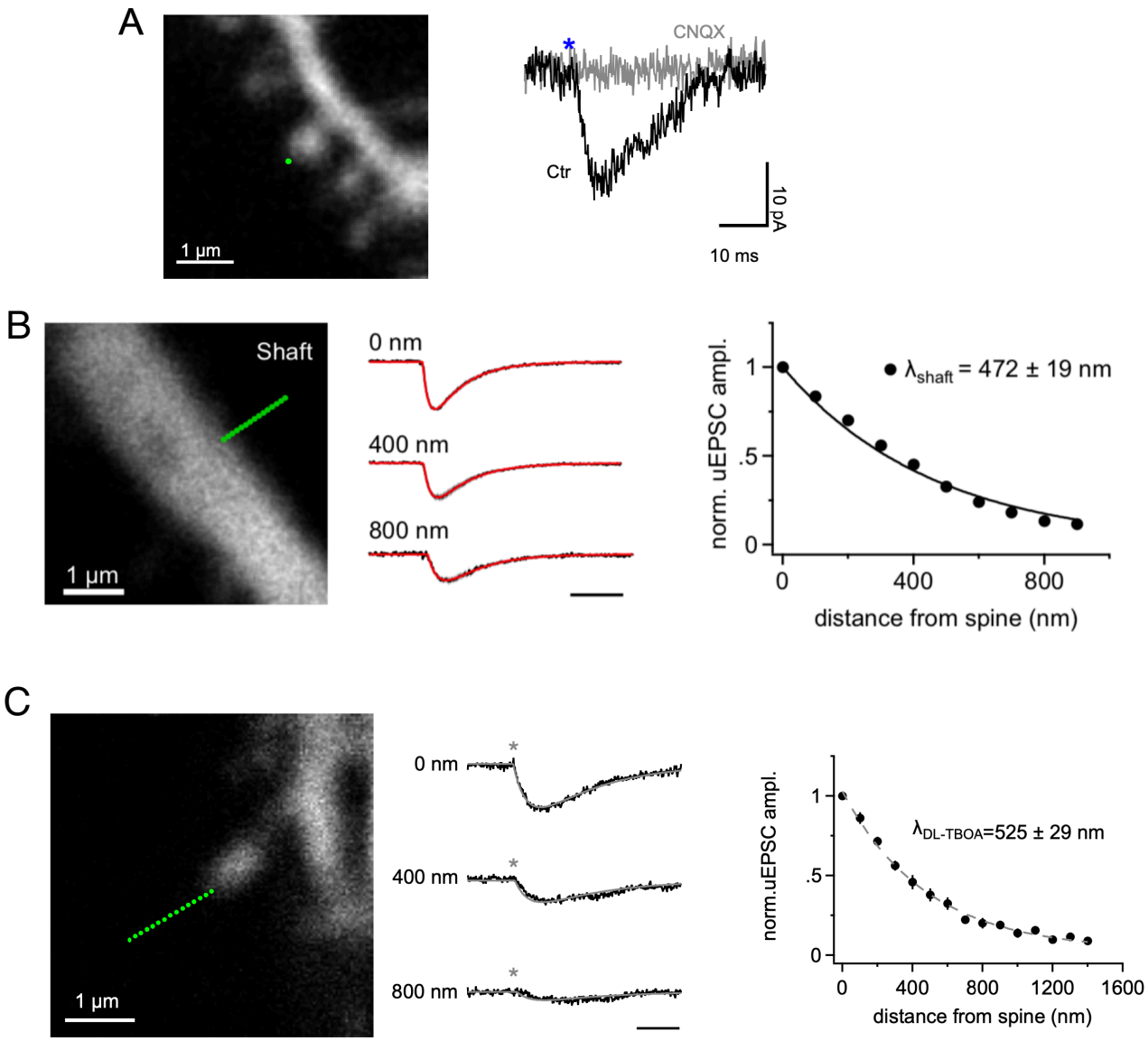

Suppl. Figure 2: uEPSCs are mediated by AMPA receptors, the apparent action range of glutamate is similar at dendritic shafts and weaker blockade of transporters shows a mild increase in the action range.

(A) Uncaging EPSCs (uEPSCs) were mediated through AMPA receptors. A single uncaging spot placed on the edge of the spine head (green dot, upper panel) while NMDA receptors were blocked by 25 µM APV in the bath, elicited an AMPA-mediated uEPSC similar to miniature EPSCs (black trace, lower panel). The blue asterisk indicates the time of the uncaging pulse. After applying 20 µM CNQX in the bath, the same uncaging pulse did not elicit any response at the same spine (grey trace, lower panel, n = 5).

(B) Apparent action range at dendritic shaft-located AMPA receptors, λ_{shaft}, equals the values measured at spine heads, suggesting the the spatial action of glutamate is determined by the surrounding neuropil and not by the type or location of the postsynaptic site. The precision of positioning the uncaging laser spot and the accuracy of the mutual alignment of both scanning systems (imaging and uncaging) was experimentally verified (Suppl. Fig. 3), scale bar, 10 ms, responses peak normalized.

(C) Glutamate uncaging in the presence of the weaker glutamate transporter blocker DL-TBOA (100 µM, n=13). Partial blockade of glutamate transporters increases the action range of glutamate showing that λ_{AMPA} also is sensitive to sub-maximal reductions in the number of unoccupied transporters. Scale bar 10 ms.

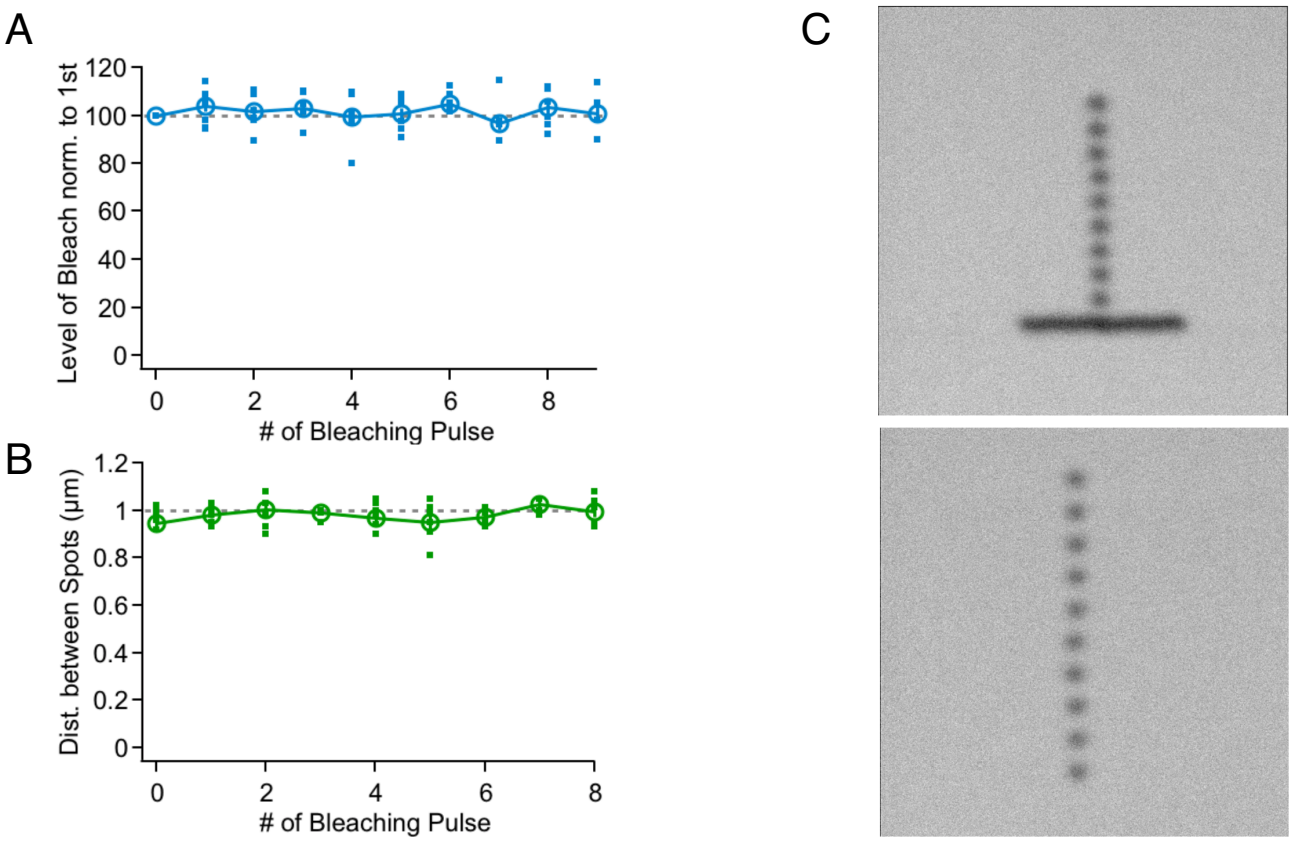

Suppl. Figure 3: Verifying reproducibility and precision of applied uncaging power and spot positioning.

(A) A plastic slide (Chroma Corp.) was used to visualize programmed uncaging events as bleached spots (cf C)). The level of bleaching as a readout of uncaging laser power was quantified in a series of uncaging spots and were constant with very little variability.
(B) Uncaging spots were positioned at nominally 1 µm intervals (C) lower panel) and image analyses of a scan of a bleached plastic spot revealed the high precision of spot placement.
(C) Top panel: Precision of alignment of imaging and uncaging laser scanning. The horizontal line was bleached with the imaging laser and the spots were bleached with the uncaging laser. Note that the first uncaging spot is precisely found on the „imaging line“. Bottom panel: Precision of uncaging laser spot positioning. 10 uncaging spots were placed at 1 µm intervals. For analysis gaussians were fitted to the bleaching profiles with sub-pixel resolution to obtain their position accurately. Distance between spots is displayed in B).

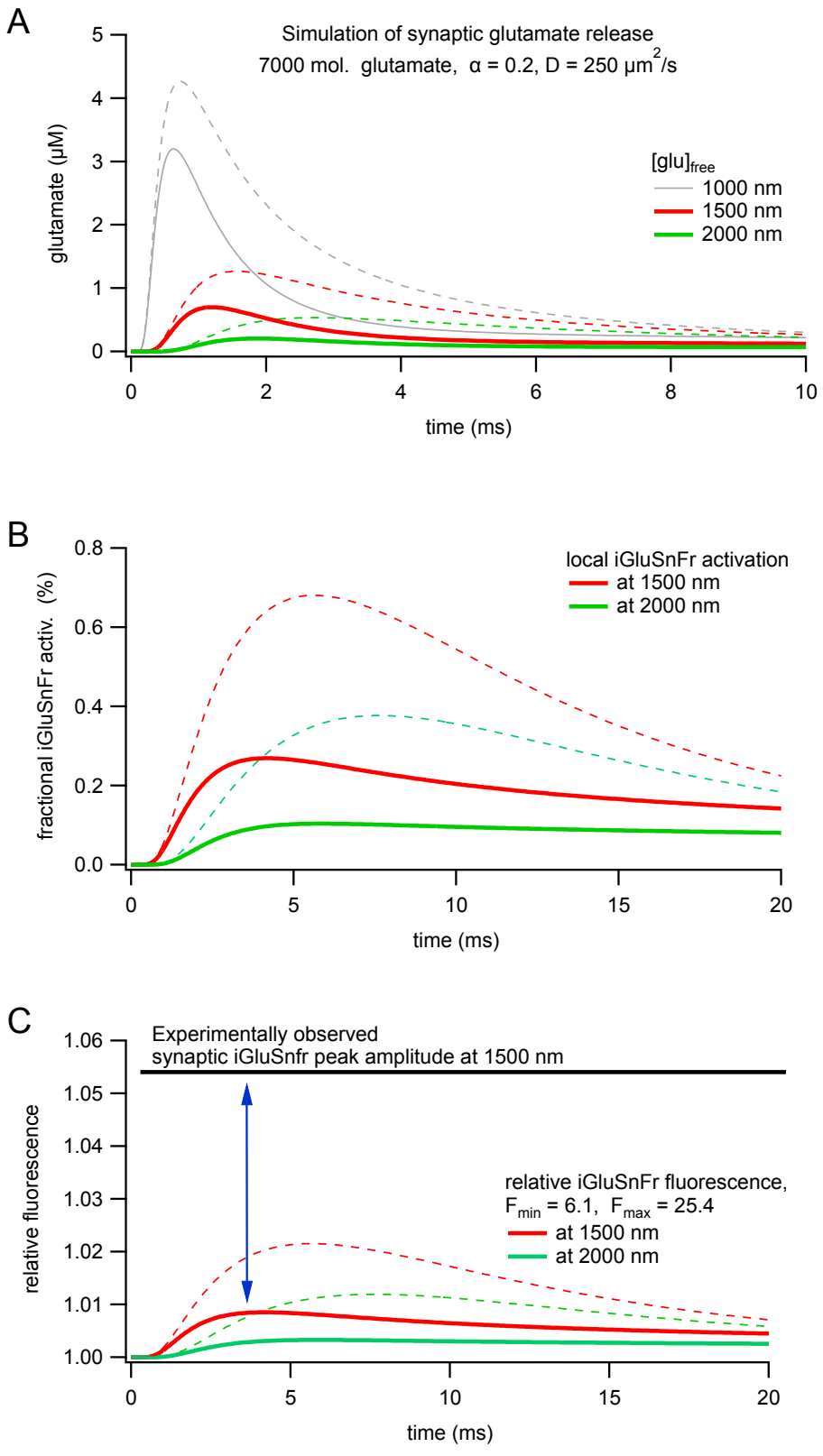

Suppl. Figure 4: Modeling iGluSnFr activation following synaptic glutamate release - comparison to experiment

(A) The simulation environment „calc“ (*V. Matveev, A. Sherman, R. S. Zucker, Biophysj. 83, 1368–1373 (2002)*) (as „spherical symmetry“) was used to replicate the neuropil diffusion models of (*D. A. Rusakov, D. M. Kullmann, J. Neurosci. 18, 3158–3170 (1998), B. Barbour, Journal of Neuroscience. 21, 7969–7984 (2001)*) and to simulate synaptic glutamate release, binding to iGluSnFr and fluorescence activation of iGluSnFr. A gaussian-shaped, fusion pore-like source of glutamate (FWHM 5 nm) was placed at the origin and glutamate was released in a peak-like fashion according to: t * sigma^2 * exp(-sigma*t) (t in ms, sigma=39), following (*D. A. Rusakov,*

D. M. Kullmann, J. Neurosci. 18, 3158–3170 (1998)). Glutamate transporters were modeled by omitting the translocation step as fixed glutamate „buffers“ at a concentration of 100 µM in the extracellular volume. Omitting the translocation is justified as it is slow and has a negligible effect on free glutamate (not shown, also see B. Barbour, Journal of Neuroscience. 21, 7969–7984 (2001)). No pre- or postsynaptic structures around the release were modeled as previous studies showed that at the distances considered here (>1000 nm) they have almost no effect on the glutamate concentration. Continuous lines throughout this figure represent calculations in the presence of glutamate „buffers“ (k+ = 5e06 /(Ms), k- = 100/s), dashed lines in their absence. An effective glutamate diffusion coefficient D=250µm^2/s was employed to account for the tortuousity of the neuropil similar to (*D. A. Rusakov, D. M. Kullmann, J. Neurosci. 18, 3158–3170 (1998), B. Barbour, Journal of Neuroscience. 21, 7969–7984 (2001)*). The vesicle contained 7000 molecules of glutamate according to recent estimates (see discussion for details).

Note that at distances of ≥1500 nm free glutamate concentrations remain below 1 µM, show a slowed rise and peak with at least 1 ms delay.

(B) The fraction of iGluSnFr molecules reaching the fluorescent state after synaptic release at 1500 and 2000 nm distance from the release site remained below 0.3%. In other words, classical neuropil diffusion models predict minimal iGluSnFr responses. We modeled iGluSnFr according to (*M. Armbruster, C. G. Dulla, J. S. Diamond, eLife. 9, 10404–26 (2020)*) with 3 states: no glutamate bound, glutamate bound and non-fluorescent and glutamate bound and fluorescent. Rate constants were also taken from that study.

(C) Conversion of fractional sniffer activation to fluorescent signals using the fluorescence constants for activated and non-activated iGluSnFr molecules indicated (taken from (*M. Armbruster, C. G. Dulla, J. S. Diamond, eLife. 9, 10404–26 (2020)*)). Note that the predicted DF/F iGluSnFr signals remain below 1%, whereas we experimentally determined iGluSnFr amplitudes at a distance of 1500 nm to be ~5.4% (black horizontal line) following spontaneous, putative quantal, release events. The blue arrow denotes the almost 5-fold differences between the experimental observation and theoretical prediction.

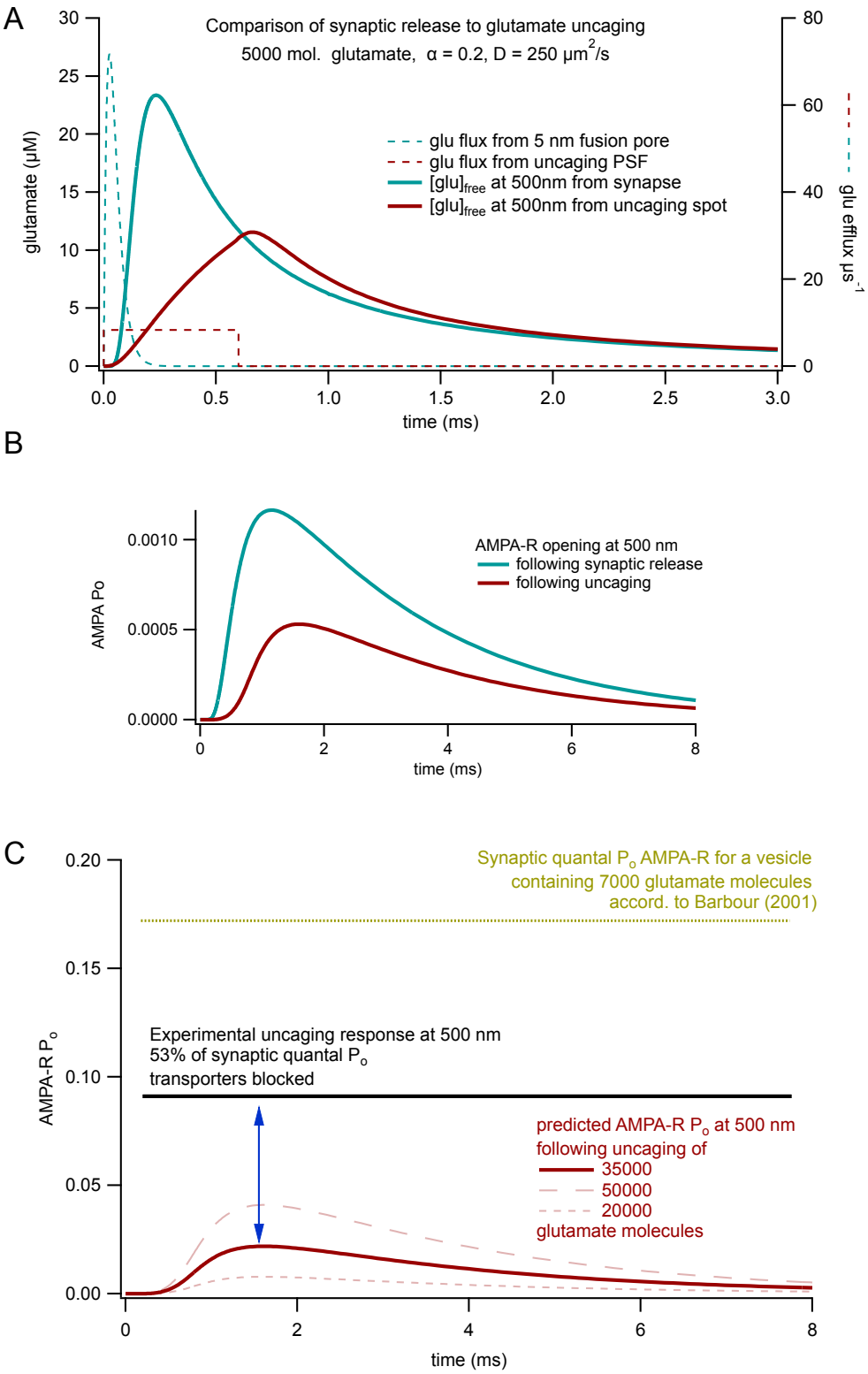

Suppl. Figure 5: Modeling AMPA-R activation following glutamate uncaging - comparison to experiment

(A) As above the simulation environment „calc“ (*V. Matveev, A. Sherman, R. S. Zucker, Biophysj. 83, 1368–1373 (2002)*) was used to replicate neuropil diffusion here in „cylindrical“ mode. Neuropil and diffusion properties as in Suppl Fig. 4. This panel compares synaptic glutamate release from a gaussian-shaped, fusion pore-like source of glutamate (FWHM 5 nm) to glutamate released from a PSF. The dashed lines indicate the flux/release rate of glutamate. In this panel, we simulated the release of 5000 glutamate molecules to facilitate comparison to previous work (*B. Barbour, Journal of Neuroscience. 21, 7969–7984 (2001)*). The peak-like release is identical to the one used for Suppl. Fig. 4, 0.6 ms of constant glutamate release was assumed for glutamate uncaging. The source of uncaging glutamate release was assumed to

be a 3D gaussian with an x-y FWHM of 280 nm and a 3.5-fold larger FWHM in the z dimension. The blue and red traces illustrate the resulting free glutamate concentration at 500 nm distance. Note that after synaptic release free glutamate rises much quicker and achieves a substantially higher peak glutamate concentration when compared to continuous 0.6 ms release during uncaging.

(B) AMPA-R opening is much lower following uncaging release of 5000 molecules of glutamate. AMPRA-R opening was modeled at a distance of 500 nm according to (*D. A. Rusakov, D. M. Kullmann, J. Neurosci. 18, 3158–3170 (1998), B. Barbour, Journal of Neuroscience. 21, 7969–7984 (2001)*). AMPA-R open probability following synaptic release compares well to (*B. Barbour, Journal of Neuroscience. 21, 7969–7984 (2001)* Fig. 4 therein).

(C) Experimentally observed AMPA-R open probabilities in response to uncaging exceed modeling prediction by at least a factor of four. The yellow dashed line indicates the open probability of synaptic AMPA-Rs according to (*B. Barbour, Journal of Neuroscience. 21, 7969–7984 (2001)*). Note that this represents a lower limit when comparing to other modeling studies eg (*D. A. Rusakov, D. M. Kullmann, J. Neurosci. 18, 3158–3170 (1998)*). No glutamate transporters were included here. The black line represents the level of AMPA-R activation we experimentally observed following glutamate uncaging at a distance of 500 nm in the presence of tfb-TBOA. The red line shows in comparison the modeled AMPA-R opening following PSF-shaped uncaging release of 35000 molecules of glutamate (calibrated uncaging content, ~5 vesicles). Even the release of 50000 molecules of glutamate would be predicted to cause a substantially lower AMPA-R activation (red dashed line). The blue arrow denotes the 4-fold differences between the experimental observation and theoretical prediction.